

# An Adaptive Contact Model for Simulation of Wheel-rail Impact Load due to a Wheel Flat

J. J. Zhu, A. K. W. Ahmed\*, S. Rakheja

Department of Mechanical and Industrial Engineering, Concordia University, Montreal, Canada

\* Corresponding author (email: waiz@vax2.concordia.ca)

## Abstract

Several reported studies have concluded that wheel-rail impact load due to a wheel flat predicted by commonly used Hertzian contact model underestimates the impact force due to a wheel flat between wheel and rail at low speeds and yields an overestimation at high speeds. In this study, an adaptive wheel-rail contact model with radial spring is developed for prediction of wheel-rail normal contact force. This proposed model adapts the contact length, contact depth and incorporates possible partial and asymmetry of the contact due to defective wheel profile. A vehicle-track interaction model incorporating a 2-D roll-plane vehicle, 3-D Timoshenko track system coupled by the adaptive contact model is developed to investigate the impact force between the wheel and rail due to a single wheel flat. The simulation results were compared with those using Hertzian contact model and available field test data. The results demonstrate the effectiveness of the adaptive contact model in predicting wheel rail impact load due to a wheel flat in a wide speed range.

**Keywords:** Adaptive Contact, Wheel-rail, Wheel Flat, and Impact Load

## 1 Introduction

Heavy haul freight cars generate significant force at the wheel-rail interface, which is further magnified when there is a defect in the wheel or rail profile. The rolling contact mechanism is a complex problem and has attracted numerous investigations in the past few decades. In the mathematical modeling and simulation of railway vehicle-track dynamics, it is the contact model that couples the vehicle system with track system. An accurate description of contact force between the wheel and the rail is thus a necessary condition to obtain reliable simulation results for the vehicle-track system. The most widely used vertical contact model is based on Hertzian non-linear elastic contact theory, which describes the contact behavior of two cylinders. Such contact model is essentially a point contact model based on the assumption that the contact patch is very small [1]. It is further assumed that the contact point

lies on the centerline of the wheel. This is a reasonable assumption in modeling vertical contact forces between a perfect wheel and rail geometry. However, when there is a defect on the wheel or rail in the contact zone, the induced impact force predicted using Hertzian contact model may not be very reliable. A few studies have suggested that the Hertzian non-linear point contact model incorporating linear track model consistently underestimates wheel flat-induced impact loads at low speeds, while overestimates at high speeds [2].

Multipoint contact model has also been proposed to predict contact forces between wheel and rail with a defect such as a wheel flat [3]. Such a model, however, assumes that the vertical contact springs are discretely and symmetrically distributed about the vertical center line of wheel regardless of perfect or defective wheel and rail profile. In the wheel-rail vertical contact study [3], it has been shown that multipoint contact model estimates impact force very similar to that of Hertzian contact model. It is not difficult to visualize that in the presence of a defect, such as a wheel flat, the radial springs will not be symmetrically distributed about the vertical center line of wheel when the region with flat enters or leaves the contact area.

For the present investigation of impact forces due to wheel flats, an adaptive wheel-rail continuous contact model is developed to overcome the limitation of the published models described above. The proposed model considers the contact length, contact depth, and possible partial contact due to defective wheel/rail profile. This adaptive contact model is based on the concept of continuous radial springs uniformly distributed over an adaptive wheel-rail footprint, which has been successfully utilized in study of ground vehicle contact problems associated with pneumatic tires [4].

The adaptive contact model developed for wheel-rail vertical interaction neglects the lateral and longitudinal forces. It is also assumed that the contact patch is very small and does not exceed the length of the flat. Due to conical or worn profile of the railway wheel, wheel radius at the contact point always varies as the wheel rolls along the track. It is however, assumed that such variations due to possible lateral motion is small and that there is no slip between the wheel and rail. The adaptive contact mode is used in this investigation to couple a 6 DOF 2-D roll plane vehicle model with 3-D rail system modeled as continuous Timoshenko beam. The simulation results in term of wheel-rail impact force due to a wheel flat are obtained using central finite difference method for different forward

velocity. The results are compared with reported analytical and field test data over a wide speed range.

## 2 Development of an Adaptive Wheel-rail Contact Model

### 2.1 Contact Force for Perfect Wheel Profile

The wheel-rail vertical interaction is represented by continuously distributed radial springs that take into account the stiffness of the wheel and the rail. As shown in Figure 1, the contact patch is designated by contact length  $l_c$ . The radially distributed springs are assumed linear, while the constant radial spring stiffness  $K_w$ , is defined as the magnitude of force required to produce unit angular deformation of the spring. The contact force is developed by radial interpenetration of the wheel into the rail. The elemental radial deflection,  $\delta_i$ , at an angle  $\alpha_i$ , leads to radial spring force  $dF$  as shown in Figure 1, such that:

$$dF = (K_w d\alpha_i) \delta_i \quad (1)$$

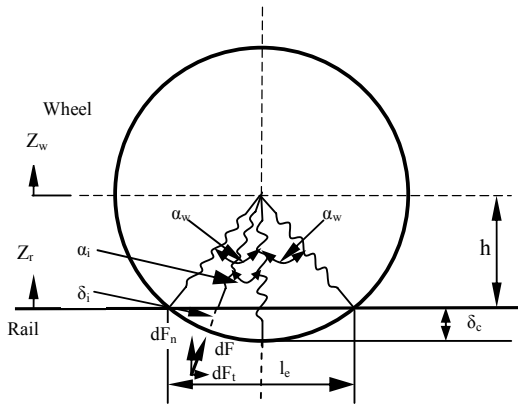


Figure 1: Radial contact representation of wheel-rail interactions

where  $\alpha_i$  is the angle between the vertical centerline of wheel plane and arbitrary contact point within the contact length. For an instantaneous wheel radius  $R_i$ , the elemental radial deflection  $\delta_i$  can be expressed as:

$$\delta_i = R_i - \frac{h}{\cos \alpha_i} \quad (2)$$

where  $h$  is distance between the wheel center and the contact patch center, given by:

$$h = R_w - \delta_c \quad (3)$$

where  $R_w$  is nominal wheel radius and  $\delta_c$  is the wheel-rail deflection at contact patch center, or the wheel rail contact overlap.

The normal and tangential components of the contact force, shown in Figure 1, can be expressed as:

$$\begin{aligned} dF_n &= (K_w \delta_i \cos \alpha_i) d\alpha \\ dF_t &= (K_w \delta_i \sin \alpha_i) d\alpha \end{aligned} \quad (4)$$

Upon combining equations (2) to (4) and integrating over the entire contact patch ( $-\alpha_w, \alpha_w$ ), the resultant wheel-

rail normal contact force with perfect contact profile can be expressed as:

$$P = F_n = 2K_w R_w (\sin \alpha_w - \alpha_w \cos \alpha_w) \quad (5)$$

where  $\alpha_w$  is wheel-rail contact patch angle, which is defined as half of the angle formed by a line connecting wheel center to the front contact point, and a line connecting the wheel center to the rear contact point. A symmetric contact about the wheel center line is assumed for a defect free wheel. The contact angle can thus be expressed as:

$$\alpha_w = \cos^{-1} \left( \frac{R_w - \delta_c}{R_w} \right) \quad (6)$$

The contact overlap  $\delta_c$  can be determined from wheel center displacement  $z_w$  and corresponding rail displacement  $z_r$ , such that:

$$\delta_c = \begin{cases} z_r - z_w & z_r - z_w > 0 \\ 0 & z_r - z_w \leq 0 \end{cases} \quad (7)$$

From the above relationships, when the overlap  $\delta_c$  and the contact force are equal to zero, the wheel contact angle is also zero. In this study, it is assumed that the rail wheel vertical displacements ( $z_r, z_w$ ) are equal to zero when the wheel and the rail are just about to come into contact.

### 2.2 Contact Force for Defective Wheel Profile

The contact model is extended to include a defect in the wheel profile in the form of a flat. As shown in Figure 2, the presence of a wheel flat could yield a contact patch that is asymmetric about the wheel centerline. For the contact patch defined by ( $\alpha_f, \alpha_r$ ), combination of equations (2) to (4) and integration over the contact patch ( $\alpha_f, \alpha_r$ ), yields resultant normal contact force as:

$$P = F_n = \int_{\alpha_r}^{\alpha_f} K_w \left( R_i - \frac{R_w - \delta_c}{\cos \alpha_i} \right) \cos \alpha_i d\alpha_i \quad (8)$$

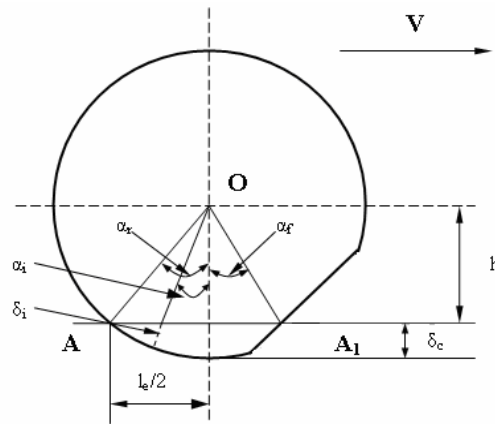


Figure 2: Deflection of an element of wheel-rail contact patch with defective wheel

where  $\delta_c$  can be calculated from equation (7);  $R_i$  is the instantaneous radius of the wheel at a position  $\alpha_i$ ;  $\alpha_f$  and  $\alpha_r$  are positions of the extreme front and rear contact point. From equation (8), it can be seen that computation of wheel-rail contact force requires: (i) determination of instantaneous wheel radius  $R_i$  at any point of contact zone; (ii) determination of the contact patch, or front and rear contact angles ( $\alpha_f$  and  $\alpha_r$ ) at every instant; and (iii) establishment of radial spring constant  $K_w$ .

### 2.2.1 Determination of the Radius $R_i$ at Arbitrary Point of Wheel Rim with a Flat

The profile of a wheel with a flat can be described by its radius and corresponding angle  $\beta$  between a reference line and the radius, as shown in Figure 3. The flat is designated by line  $BB_1$  and the reference is chosen as the vertical line through wheel center. The initial position of the flat is described by the angle between the reference line and the wheel flat center line ( $\beta_0$ ). The length of the flat is determined by arc angle  $\varphi$ , which represents half of the chord angle between  $OB$  and  $OB_1$ . For a small flat length, this arc angle can be expressed as:

$$\varphi = \frac{l_f}{2R_w} \quad (9)$$

where  $l_f$  is the length of flat and  $R_w$  is the nominal wheel radius. The instantaneous radius of wheel at arbitrary position can now be simply expressed by:

$$R_i = \begin{cases} R_w & 0 < \beta \leq \beta_0 - \varphi \text{ OR } \beta_0 + \varphi < \beta \leq 2\pi \\ R_w - f & \beta_0 - \varphi < \beta \leq \beta_0 + \varphi \end{cases} \quad (10)$$

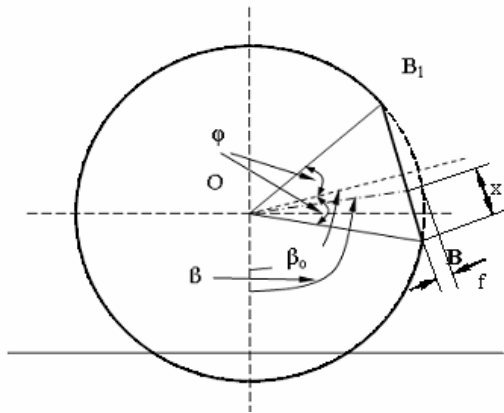


Figure 3: Wheel profile with a flat

where  $f$  is the variation in the wheel radius due to wheel flat, and is dependent upon the type of flat being considered. When the wheel flat is just formed, it takes the form of a chord. It is often referred to as “fresh flat” or “chord flat”. For fresh or chord type flat,  $f$  can be obtained by the geometry of the profile, such that:

$$f = R_w - \frac{R_w - D_f}{\cos(\beta - \beta_0)}, \quad \beta_0 - \varphi < \beta \leq \beta_0 + \varphi \quad (11)$$

$$D_f = R_w - \sqrt{R_w^2 - \frac{l_f^2}{4}} \quad (12)$$

In practice, the two ends of “chord” become rounded due to continuous running on the rail. This type flat is usually called “rounded flat”, or “worn flat”, or “haversine flat”. The variations in the radius due to such a flat,  $f$ , can be described by [5]:

$$f = 0.5 D_f \left[ 1 - \cos\left(\frac{2\pi x}{l_f}\right) \right] \quad (13)$$

where  $D_f$  is the depth of flat and can be estimated using following equation if it is unknown [5]:

$$D_f = \frac{l_f^2}{16 R_w} \quad (14)$$

The term  $x$  in equation (13) is the distance between an arbitrary point on the flat and the front end of the flat (des-

ignated by  $x$  in Figure 3), and can be expressed in terms of angle  $\beta$ , such that:

$$x = \frac{l_f}{2} + (R_w - D_f) \tan(\beta - \beta_0), \quad \beta_0 - \varphi < \beta \leq \beta_0 + \varphi \quad (15)$$

The instantaneous wheel radius can be then obtained as a function of position  $\beta$  by substituting for  $f$  into equation (10). In this study, only the haversine flat model is used to represent a flat with a given length and depth since this model is more commonly used and such type of flat is more commonly observed in practice.

The position of the wheel flat with reference to vertical centerline of wheel would vary as the wheel rotates. Figure 4 shows the flat position at an instant  $t$ , where the flat has shifted by an angle  $\gamma$  from the initial position. For a constant forward speed  $V$ , the angle  $\gamma$  can be expressed as:

$$\gamma = \omega t = \frac{V}{R_w} t \quad (16)$$

The corresponding new position of flat is then given by  $\beta_0 - \gamma$ . By substituting  $(\beta_0 - \gamma)$  for  $\beta_0$  in equations (15), (11) and (10), the instantaneous wheel radius  $R_i$  at any point including contact zone can be readily obtained for a rotating wheel. For a haversine type flat,  $f$  can be determined from equation (13) by substituting for  $x(t)$ , given by:

$$x(t) = \frac{l_f}{2} + (R_w - D_f) \tan[\beta(t) - (\beta_0 - \gamma(t))]; \quad (\beta_0 - \gamma(t)) - \varphi < \beta(t) \leq (\beta_0 - \gamma(t)) + \varphi \quad (17)$$

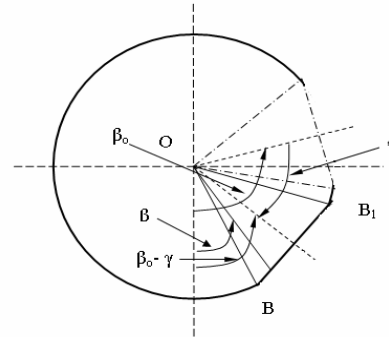


Figure 4: Scheme of a rotating wheel with a flat

Figure 5 shows the variation in wheel radius at the contact patch center when rolling at a speed of 50 km/h. For this case the wheel and the flat are defined by:  $R_w = 0.4572$  m,  $l_f = 100$  mm,  $D_f = 1.5$  mm and  $\beta_0 = 90^\circ$ .

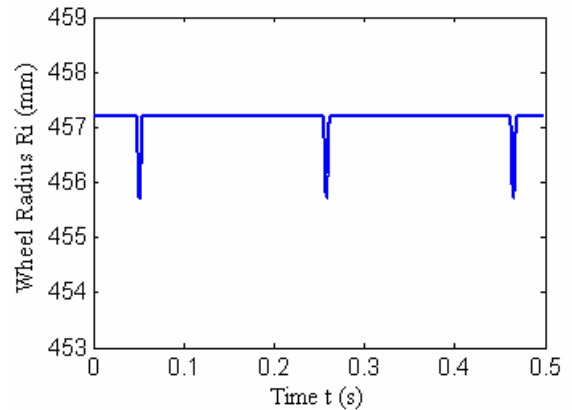


Figure 5: Changes in effective rolling radius of a rotating wheel with a flat

### 2.2.2 Determination of the Contact Patch ( $\alpha_f, \alpha_r$ )

As illustrated earlier in Figure 2, a wheel flat would yield asymmetric contact geometry about the vertical wheel centerline. The analysis of this geometry involves identification of the wheel-rail contact patch, or the extreme front and rear contact angles ( $\alpha_r, \alpha_f$ ) in the presence of a flat, as shown in Figure 6. The figure also shows the contact geometry for perfect wheel, which is described by angle  $\pm\alpha_w$ . The contact geometry is derived upon consideration of the displacements of wheel and rail, which yield overlap  $\delta_c$  using equation (7). Furthermore, the instantaneous radius of wheel rim  $R_i$  is derived from equation (10). The positions of the front and rear contact point position ( $\alpha_f, \alpha_r$ ) are derived from the corresponding radii  $R(\alpha_f)$  and  $R(\alpha_r)$ , such that:

$$\begin{aligned} R(\alpha_f) \cos(\alpha_f) &= R_w - \delta_c \\ R(\alpha_r) \cos(\alpha_r) &= R_w - \delta_c \end{aligned} \quad (18)$$

Within the contact patch:

$$R(\alpha_i) \cos(\alpha_i) > R_w - \delta_c \quad (19)$$

And outside the contact patch:

$$R(\alpha_i) \cos(\alpha_i) < R_w - \delta_c \quad (20)$$

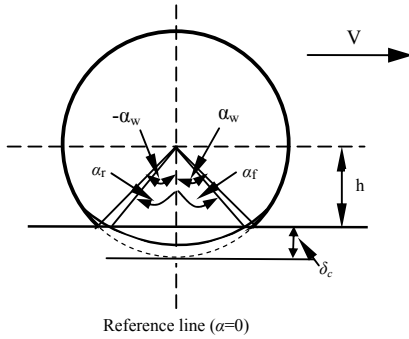


Figure 6: Identification of wheel rail contact patch ( $\alpha_f, \alpha_r$ ) in specified co-ordinate system

Above formulations suggest that an iterative approach can be adopted to verify the contact patch coordinates. Assuming a defect free wheel profile, contact patch angles are initially taken as  $-\alpha_w, \alpha_w$ . The wheel radii  $R_i$  at every point within  $\alpha_w$  are computed until the extreme contact points are established using the above requirements.

### 2.2.3 Establishment of Wheel-Rail Contact Radial Spring Stiffness

The effectiveness of the proposed adaptive contact model is largely dependent on the identification of reliable value for the radial spring constant  $K_w$ . Although experimental characterization would be desirable, an estimate of  $K_w$  may be obtained from analysis of wheel-rail interpenetration under a static load  $P_o$ . Rewriting equation (5) yields an expression for the stiffness  $K_w$ :

$$K_w = \frac{P_o}{2 R_w (\sin \alpha_w - \alpha_w \cos \alpha_w)} \quad (21)$$

where  $\alpha_w$  can be determined from equation (6).

The static wheel rail overlap  $\delta_o$  should be ideally determined by experimentally measuring the static displacement of rail and wheel center. Alternatively it can be de-

rived from the Hertzian non-linear contact theory by assuming that the contact patches calculated from the two different models is same under the same static load. Hertzian contact theory provides following relationship between applied load and wheel-rail overlap [1]:

$$P = C_H \delta^{\frac{3}{2}} \quad (22)$$

where  $\delta$  is the overlap between wheel and rail; and  $C_H$  is the Hertzian contact coefficient. The above relationship can also be applied to determine static overlap of wheel and rail,  $\delta_o$ , by assuming the contact force as the static load  $P_o$ .

## 3 Vehicle-track Interaction model

The magnitudes of impact forces caused by wheel defects are strongly dependent upon vertical dynamics of the coupled vehicle-track system. The analysis of wheel-rail contact force response thus necessitates development of a representative vehicle-track system model incorporating the contact model. In this work, the adaptive wheel rail contact model is applied to a three dimensional model of multiple layers track system in conjunction with roll plane model of the vehicle system. Such formulation permits for analysis of the influence of a wheel defect on the wheel-rail interaction of not only the defective wheel but also the other wheel within the same axle.

The simplified vehicle model consists of half bolster coupled to two half-sideframes through the secondary suspension and a complete wheelset as shown in Figure 7. The various degrees of freedom include: the bounce ( $z_b$ ) and roll ( $\phi_b$ ) motions of the bolster; bounce motions of the left and right sideframes ( $z_{sfl}, z_{sfr}$ ); and the bounce ( $z_w$ ) and roll ( $\phi_w$ ) motions of the wheelset.

The elements of primary suspension represented by  $K_1, C_1$  and secondary suspension represented by  $K_2, C_2$  are assumed to be linear. Load  $W$  stands for a quarter of car body weight, and acts on the center of the bolster.  $P_l$  and  $P_r$  are vertical forces at the wheel-rail contacts at the left and right wheels, respectively. The model neglects interactions between the leading and trailing wheelsets within a bogie. The contributions of the car body dynamics are also considered to be relatively small due to its low natural frequency. The equations of motions of roll-plane vehicle model are expressed in the matrix form as follows:

$$[M]\{\ddot{d}\} + [C]\{\dot{d}\} + [K]\{d\} = \{F\} \quad (23)$$

Where  $[M]$ ,  $[C]$  and  $[K]$  are mass, damping and stiffness matrix, respectively; and vector  $\{d\}$  is the displacement vector;  $\{F\}$  is the generalized external force vector.

For a roll plane vehicle model, it is necessary to consider a pair of rail system in three-dimension (3-D). For this investigation, two-layer track system model consisting of left and right rails, pads, sleepers and ballast elasticity is developed, as shown in Figure 8. Two rails are modeled as Timoshenko beams supported on the sleepers modeled as lumped masses, through the rail-pads and fasteners that are represented by springs and dampers. The ballast is modeled as springs and dampers inserted between each discrete sleeper and subgrade.

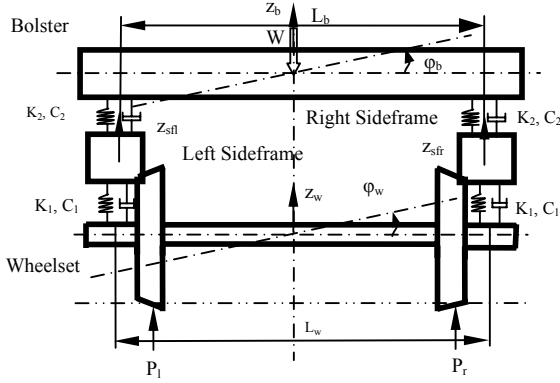


Figure 7: Six-DOF roll-plane vehicle model

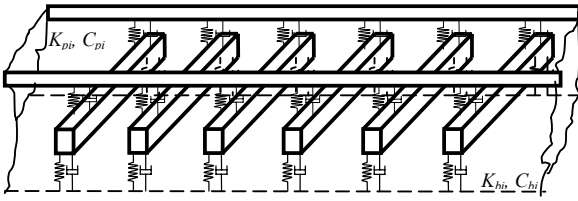


Figure 8: Schematic of the two-layer 3D track system

A rail of length  $L$ , modeled as Timoshenko beam supported discretely by ‘ $n$ ’ sleepers is shown in Figure 9. Both ends of the rail are assumed fixed, where ‘ $a$ ’ denotes the spacing between two adjacent sleepers.  $P_c$  and  $X_w$  represent the vertical contact load and its location along the rail length. For the rail model with a moving point load  $P_c$  and discrete support forces  $F_i$  (Figure 9), the governing equations for vertical and bending motions can be expressed as [6]:

$$\begin{aligned} \frac{\partial}{\partial x} \left\{ kAG \left[ \frac{\partial Z_{Rl(r)}(x,t)}{\partial x} - \theta_{l(r)}(x,t) \right] \right\} - \bar{m} \frac{\partial^2 Z_{Rl(r)}(x,t)}{\partial t^2} &= P_{cl(r)}(t) \delta(x - X_w) - \sum_{i=1}^n F_{il(r)} \delta(x - ia) \\ \frac{\partial}{\partial x} \left[ EI \frac{\partial \theta_{l(r)}(x,t)}{\partial x} + kAG \left[ \frac{\partial Z_{Rl(r)}(x,t)}{\partial x} - \theta_{l(r)}(x,t) \right] \right] - \bar{m} r^2 \frac{\partial^2 \theta_{l(r)}(x,t)}{\partial t^2} + P_a \theta_{l(r)}(x,t) &= 0 \end{aligned} \quad (24)$$

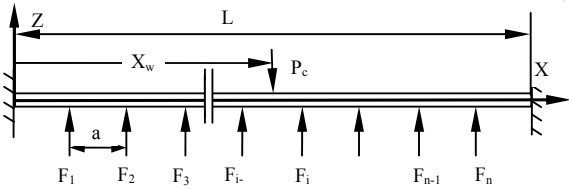


Figure 9: Model of rail supported by sleepers (fixed end)

where  $Z_R$  and  $\theta$  represent rail vertical and rotational motions;  $k$  is the shear coefficient of rail;  $A$  is the cross-sectional area of the rail and  $G$  is the shear modulus of the rail material;  $EI$  represents the flexural rigidity of the rail.  $\delta$  function represents the position of vertical forces on the rail and converts the concentrated forces into distributed forces. Subscript  $i$  refers to  $i^{\text{th}}$  sleeper, and notation  $l(r)$  refers to left (right) side rail.  $\bar{m}$  is rail mass of unit length.  $r$  is the radius of gyration of rail cross-section.  $P_a$  is longitudinal force applied on the rail which is neglected in this study.

As shown in Figure 8, the sleepers are model as lumped masses. A set of springs and dampers represent the compliance of the ballast. The lateral distance between two rail supports is  $L_s$ . The vertical displacement  $Z_{is}$  and roll displacement  $\phi_{is}$  of  $i^{\text{th}}$  sleeper due to rail pad force  $\{F_s\}$  are derived from the following differential equation:

$$[M_s] \{\ddot{d}_s\} + [C_s] \{\dot{d}_s\} + [K_s] \{d_s\} = \{F_s\}^T \quad (25)$$

where  $[M_s]$ ,  $[C_s]$  and  $[K_s]$  are the mass, damping and stiffness matrices;  $\{d_s\}$  is the displacement vector. The detailed derivation of the equations is presented in [7].

## 4 Simulation Results

Coupled vehicle-track system model developed in the previous section considered the rail as continuous system, while the vehicle and sleeper components are modeled by discrete or lumped parameter systems. Mathematically, the model is represented by a set of coupled ordinary (ODE) and partial differential equations (PDE). It is essential to explore an effective method for analysis of coupled partial and ordinary differential equations with sufficient accuracy and stability of the solution. In this study, a central finite difference method (CFDM) is applied to solve for partial and ordinary differential equations [7].

In this study, a nominal wheel flat is defined as 100 mm long and 1.5 mm deep. This flat is introduced only to the left wheel, while the right wheel is assumed to have a perfect profile. The vehicle and track parameters listed in Table 1 and the above flat size are selected to facilitate a direct comparison of results with those available in the literature. Simulations are carried out for track length corresponding to 50 sleepers and results are presented for a time segment where any effect of boundary conditions is absent. Figure 10 illustrates a segment of the time history of wheel-rail contact force at the left and right wheel-rail interface for a forward speed of 70 km/h.

When the flat on left wheel comes into contact, the contact force reduces due to loss of contact as the left wheel suddenly drops while the left rail moves up until the wheel hits the rail. Thus an impact force is produced. As shown in Figure 10, there is a total loss of contact at the left wheel for the speed and flat size considered. After the impact, the contact force oscillates for about a cycle prior to dissipating due to the damping. Figure 10 further shows that the contact force at the right wheel-rail interface also varies in a similar manner. The magnitude in this case, however, is much smaller and takes places with a time delay in relation to the left wheel. For the speed and flat size considered, the impact force at the left wheel with flat is found to be more than 3.5 times the static load, whereas the peak force at the other side is about 1.5 times the static wheel load.

In order to examine the impact sequence in terms of wheel and rail motions, the time history of wheel and rail displacements is presented in Figure 11. The results show the change of wheel and rail movement at the left and right track as the vehicle runs along the track. When the flat on left wheel comes into the contact region, the left rail moves up and wheel drops down prior to impact between wheel and rail. After impact, the left wheel and rail oscil-

late around their individual static position for a short duration. Meanwhile, at the right side, both rail and wheel move up at first to compensate for the roll motion of the axle as left wheel drops due to the flat. The resulting oscillating motions of the rail and wheel at the right side yield the variation in the contact force at that wheel.

Table 1: Parameters of vehicle and track system [8]

Vehicle System	
Car body mass (quarter of vehicle)	20150 kg
Bolster mass (half)	232.5 kg
Mass moment of inertia of bolster about centerline of track (half)	87.5 kg.m <sup>2</sup>
Mass of half side frame (half)	223.75 kg
Mass of wheelsets	1120 kg
Mass moment of inertia of wheelset about centerline of track	420.1 kg.m <sup>2</sup>
Primary suspension stiffness	6.5 MN/m
Primary suspension damping coefficient	100 kN.s/m
Secondary suspension stiffness	2.55 MN/m
Secondary suspension damping coefficient	44.24 kN.s/m
Distance between left and right secondary suspension in bogie	1.6002 m
Distance between left and right wheel bearing center	1.6002 m
Wheel radius	0.475 m
Track System	
Shear coefficient	0.34
Rail cross section area	7.77×10 <sup>-3</sup> m <sup>2</sup>
Shear modulus of rail	81GN/m <sup>2</sup>
Elastic modulus of rail	2.07×10 <sup>11</sup> N/m
Second moment of area of rail about Y axis	2.94×10 <sup>-5</sup> m <sup>4</sup>
Rail mass per meter	60 kg/m
Pad stiffness	140 MN/m
Pad damping coefficient	45 kN/m
Ballast stiffness (*)	40 MN/m
Ballast damping coefficient (*)	50 kN.s/m
Sleeper mass	270 kg
Mass moment of inertia of sleeper	90 kg.m <sup>2</sup>
Sleeper spacing	0.685 m
Rail support distance (*)	1.505 m
Radial spring stiffness	3.3443×10 <sup>10</sup> N/m/radian
Note: The parameters with(*) are not given by reference [8] and assumed according to typical freight car[3]	

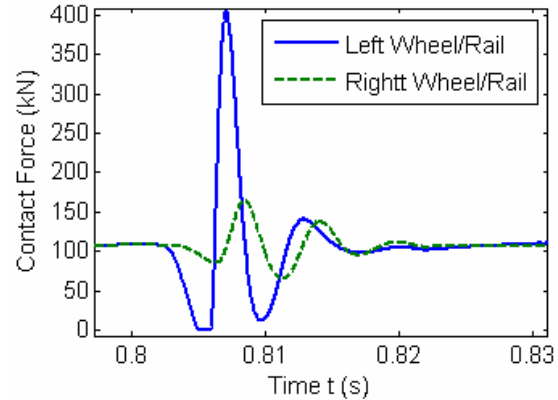


Figure 10: Contact force time history in the proximity of wheel flat contact

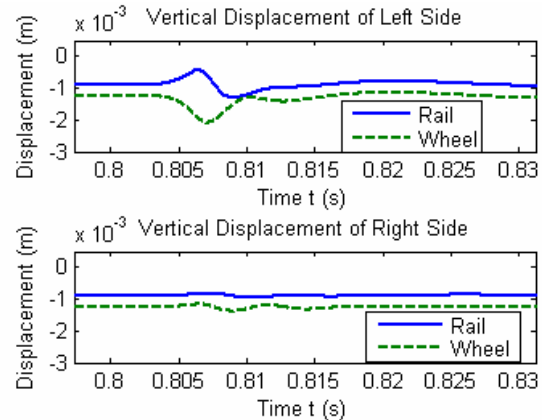


Figure 11: Time history of wheel-rail displacement

#### 4.1 Comparison with Hertzian Contact Model

The most widely used contact theory for vertical wheel-rail contact force simulation is the Hertzian contact model. One of the motivations for the present investigation was to introduce a new radial spring adaptive contact model that can accommodate asymmetric contact region for defective wheel profile. In order to compare the developed model in application to wheel flat, the vehicle-track system model incorporating Hertzian contact model and the developed adaptive contact model are simulated for identical parameters. A common value in literature used for Hertzian contact coefficient is  $c_H = 0.85 \times 10^{11}$  for Hertzian contact model, while the radial spring stiffness of the adaptive model is selected such that both models yield identical static contact force.

The simulation is carried out for a 100 mm long and 1.5 mm deep flat at a speed of 70 km/h. The contact force result for one steady-state impact cycle is shown in Figure 12. As the results show, the impact force from Hertzian contact model (558.0 kN) is significantly larger than that from adaptive model (404.7 kN). The impact force predicted by adaptive contact model is therefore 27.5% less than that from Hertzian contact model at 70 km/h for given parameters. The results in Figure 12 further show that the

Hertzian contact model predicts the loss of contact of wheel-rail second time after the impact, and the duration of the second loss of contact is even larger than the first one, which is unlikely in practice.

In order to examine the effect of speed, the peak impact load due to the same flat within the speed range 0 ~ 180 km/h is plotted in Figure 13. As the results show, both models predict similar trend for change in speed. However, in comparison to adaptive contact model, Hertzian contact model underestimates wheel-rail impact load at low speeds, and overestimates the impact load at high speeds. Such a trend for the performance of adaptive contact model is very encouraging since it is well known in the literature that for simulation of impact force due to wheel flat, Hertzian contact model may underestimate at low speeds while may overestimate at high speeds. Another noticeable difference between the two contact models as shown in Figure 13 is the fact that beyond 90km/h, the peak impact force predicted by Hertzian contact model reduces considerably as speed is increased, whereas the adaptive contact model exhibits very small reduction with increasing speed.

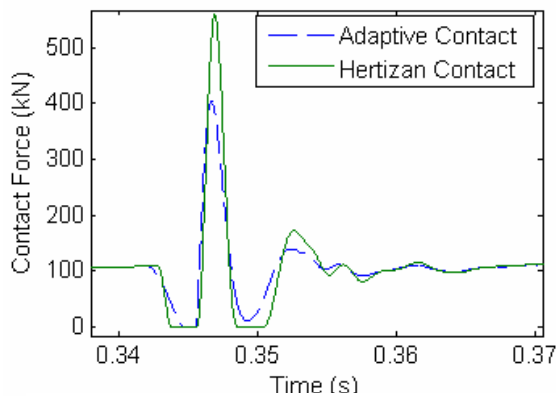


Figure 12: Comparison of contact force from adaptive and Hertzian contact model

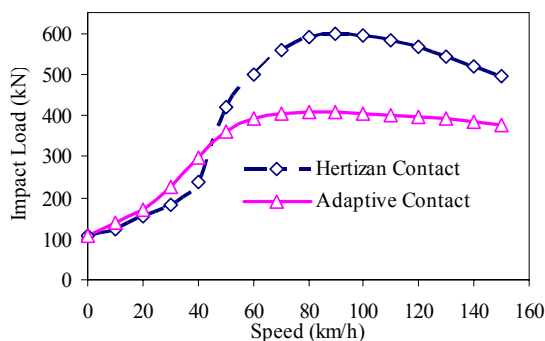


Figure 13: Comparison of wheel-rail impact load at different forward speeds

## 4.2 Comparison with Published Field Test Data

In order to investigate the influence of wheel flat on the dynamic wheel-rail contact force, the Centre of Excellence CHARMEC (CHAlmers Railway MEchanics) carried out

extensive field measurements in Svealandsbanan, Sweden on the main line between Eskilstuna and Sodertalje in co-operation with Chalmers University of Technology in 2000 [9]. The response of wheel-rail contact force due to a 100 mm long, 0.9 mm deep wheel flat was measured at different traveling speed.

The wheel rail contact force was measured utilizing an instrumented sleeper bay over which a bogie with a flat wheel was moved at different speeds. A sample of experimental time history of impact force at 50 km/h is shown in Figure 14. As the result shows, the wheel-rail contact force recorded is zero except when the wheel is on the instrumented sleeper bay. The impact sequence can be clearly identified from the result. As the wheel flat approaches contact region, there is an initial drop in the contact force from the static value. This is followed by a relatively sharp peak force referred to as the impact force. Finally the impact force is followed by a damped oscillation of the contact force as the wheel travels away from the instrumented bay. The second increase in Figure 14 corresponds to rear wheel with perfect profile entering the instrumented bay.

The experimental vehicle and track parameters and description of wheel flat (100 mm long and 0.9 mm deep) are also simulated using the developed model for this investigation. Majority of the parameters are obtained from reported studies by Anderson and Oscarsson [10] and by Nielsen and Oscarsson [2]. They also carried out numerical simulation of wheel-rail impact force response due to such wheel flat to compare with experimental results in [9]. The time history of the contact force from the current study is presented in Figure 15. The result for 50 km/h shows very good agreement with the field test result presented in Figure 14. The peak contact force (215 kN) and the trend predicted from this simulation is very similar to the peak (211 kN) and trend observed in the field test.

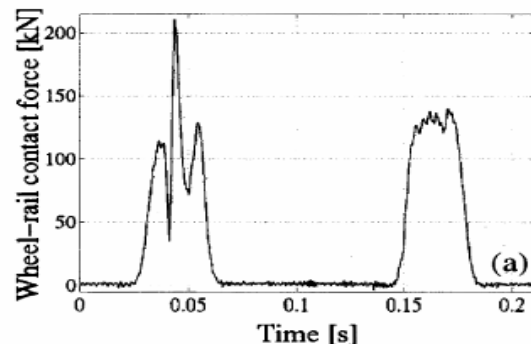


Figure 14: Time history of wheel rail contact force measured in one instrumented sleeper bay at 50 km/h [16]

The simulated peak contact or the impact load for the same parameters is evaluated for speed in the range of 5 to 100 km/h. These results are presented in Figure 16 along with experimental result from [9]. Figure 16 further presents the numerical results obtained in [2, 10] for Hertzian nonlinear contact model along with single wheel vehicle model, and linear and nonlinear track model. Although some experimental results are scattered, it is easy to see that the present vehicle-track model with adaptive contact model

shows closest trend to the experiment among all the results presented in Figure 16. Particularly, the effectiveness of the adaptive contact model as opposed to Hertzian model at high speed is highly significant.

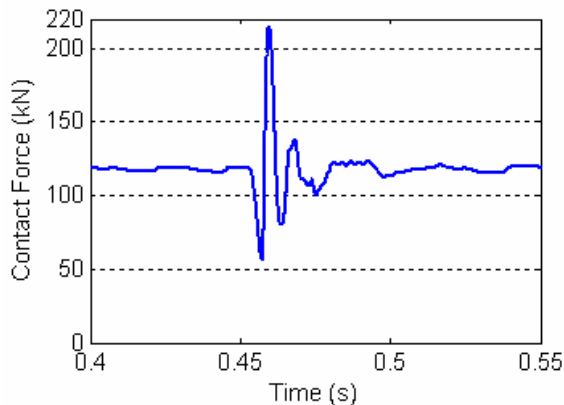


Figure 15: Time history of wheel rail contact force calculated in present simulation at 50 km/h

It is also apparent that the simulated results obtained in this investigation tend to predict the upper bounds of experimentally observed impact loads for speeds beyond 40 km/h. From the influence of nonlinearity in the track system [2] as shown in Figure 16, it is possible that the present model with track system nonlinearity may produce even a better agreement with the experimental values over the entire speed range.

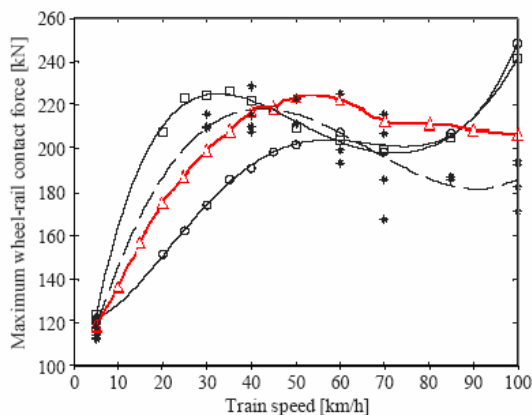


Figure 16: Comparison of impact load due to a 100 mm long, 0.9 mm deep wheel flat  
 $\Delta$ : present investigation; \* : experimental data;  $\square$ : nonlinear track model by Nielsen;  
 $\circ$ : linear track model by Nielsen

## 5 Conclusions

Unlike the single or multiple point contact models, the proposed adaptive contact model is based on continuous wheel-rail contact in the contact patch, and accounts for asymmetry of the patch and partial contact as the flat enters and leaves the contact region.

The response of the vehicle-track system in terms of contact force is examined for two different flat sizes at various forward speeds. Results are compared with reported experimental and computational data in time domain and in terms of peak impact force at different speeds.

The results demonstrate that adaptive contact model is more realistic for accurate representation of the contact between wheel and rail. The comparative study shows that the proposed model, although simplified in terms of vehicle and track systems, can predict wheel-rail impact load better than nonlinear Hertzian point contact model. This study also shows that wheel flat can cause wheel-rail impact load not only between the defective wheel and rail, but also between the rail and cross wheel. Further studies are proposed with nonlinear track model, and for establishment of accurate radial spring stiffness for adaptive contact model.

## References

- [1] Z. Q. Cai, "Modeling of rail track dynamics and wheel/rail interaction", Ph.D. Thesis, Queen's University 1992.
- [2] J.C.O. Nielsen and J. Oscarsson, "Simulation of dynamic train-track interaction with state-dependent track properties", Journal of sound and vibration, 275(2004), 515-532.
- [3] R. G. Dong, "Vertical Dynamics of Railway Vehicle-track System", Ph.D. Thesis, Concordia University 1994.
- [4] K. Wang, "Dynamic analysis of a tracked snow plowing vehicle and assessment of ride quality", MAsc. Thesis, Concordia University 1998.
- [5] D. Lyon, "The calculation of track forces due to dipped rail joints, wheel flats and rail welds". Paper presented at the Second ORE Colloquium on Technical Computer Programs, May 1972.
- [6] S. W. Weaver, *et al.*, "Vibration problems in engineering", 5<sup>th</sup> ed. Wiley, New York c1990.
- [7] J. J. Zhu, "Development of an adaptive contact model for analysis of wheel-rail impact load due to wheel flats", MAsc. Thesis, Concordia University 2006.
- [8] M. Fermer and J. C. O Nielsen, "Vertical interaction between train and track with soft and stiff railpads---full scale experiments and theory". Proc. Instn Mech.Engrs, Part F: J. Rail and Rapid Transit, 1995, 209(F1), 39-47.
- [9] A. Johansson and J. C. O. Nielsen, "Out-of-round railway wheels - Wheel-rail contact forces and track response derived from field tests and numerical simulations", Proceedings of the Institution of Mechanical Engineers, Part F: Journal of Rail and Rapid Transit, 2003, Vol: 217 Iss: 2 Page: 135.
- [10] C. Andersson and J. Oscarsson, "Dynamic train/track interaction including state-depent track properties and flexible vehicle components", Vehicle system dynamics 33, 47-58, 1999.